applied sciences

MDPI

Article

Synthesis and Characterization of Biochar-Based Geopolymer Materials

Federica Piccolo, Fernanda Andreola, Luisa Barbieri and Isabella Lancellotti *

Department of Engineering "Enzo Ferrari", University of Modena and Reggio Emilia, 41126 Modena, Italy; federica.piccolo@unimore.it (F.P.); andreola.fernanda@unimore.it (F.A.); luisa.barbieri@unimore.it (L.B.)
* Correspondence: isabella.lancellotti@unimore.it; Tel.: +39-059-2056251

Abstract: The aim of this research is to evaluate the possibility to realize alkali-activated materials exploiting biochar, a secondary raw material coming from pyrolysis/gasification processes, for environmental benefits, such as improvement of soil fertility and reduction of CO_2 emissions into the atmosphere thanks to the carbon sink process where carbon dioxide is subtracted from the cycle of carbon. For the matrix of the geopolymers, a waste material derived from incinerator bottom ash was used and compared to pure metakaolin matrix. The materials obtained are lightweight and porous, with high water absorption capacity and moisture adsorption/desorption. BET analysis shows an increase in specific surface by increasing the biochar content and the biochar acts as a filler in the pores. From porosimetry analysis it is possible to follow the evolution of the curing process of the geopolymer prepared: specimens containing 70 wt% biochar after 28 and 90 days showed an increase in total Hg intrusion volume, pore area and total porosity but a decrease in the dimensions of pores. Due to the technical properties of materials containing biochar, they can be used in the future for a cleaner design of products in the field of sustainable construction for insulating panels or lightweight materials for houses and gardens in terraces and balconies.

Keywords: geopolymer; biochar; bottom ash; lightweight material

Citation: Piccolo, F.; Andreola, F.; Barbieri, L.; Lancellotti, I. Synthesis and Characterization of Biochar-Based Geopolymer Materials. *Appl. Sci.* **2021**, *11*, 10945. https://doi.org/10.3390/app112210945

Academic Editors: Joan Formosa Mitjans and Jessica Giró Paloma

Received: 14 October 2021
Accepted: 16 November 2021
Published: 19 November 2021

1. Introduction

Vegetable biomass can be treated by combustion, gasification or pyrolysis according to the scheme reported below (Figure 1):

If the chemical oxidation between a fuel and a comburent (generally oxygen) is total, combustion takes place and thermal energy and new components are generated. For the biomass the combustion takes place in three steps: drying (water evaporation), pyrolysis-gasification (biomass degradation in the absence or partial presence of oxygen), oxidation of coal and combustible gases If the oxidation of a liquid or solid material at temperatures between 800 and 1100 °C is partial (i.e., with air in a quantity lower than the stoichiometric one), gasification is realized and the products are gases (CO, H_2, CO_2 and CH_4) with medium-low calorific value, a fraction of heavy hydrocarbons condensable at room temperature (tar) and a solid residue consisting of the inert fraction of the treated material (char). When the biomass is thermochemically decomposed by applying heat at temperatures between 400 and 800 °C, in the complete absence of oxidizing elements, or at the most, using a very small amount of oxygen (partial gasification), pyrolysis occurs. The products are: a low-medium calorific gas fraction containing CO; CO_2; hydrocarbons (CH_4, C_2H_4, C_3H_6); H_2O; H_2; an oily liquid fraction containing tar, water and low molecular weight organic compounds such as aldehydes, acids, ketones, alcohols; and a solid product consisting of residues with a higher molecular weight such as carbonaceous portions (char), ashes, inert materials and metal species.

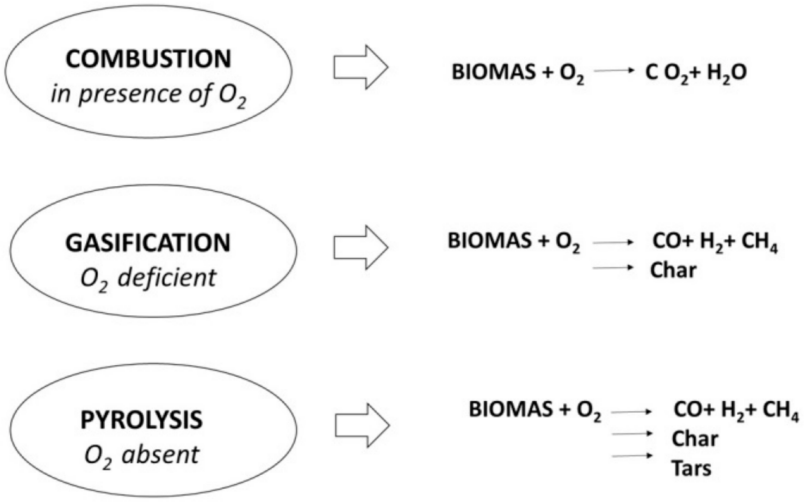

Figure 1. Scheme of combustion, gasification and pyrolysis.

Char is often used as a fuel, but it can be used for any heat generation requirement. Coal burns very hot, even hotter than the biomass from which it started and with very little smoke, making it excellent as a fuel. Biochar is very similar to char but has an intended use as a soil amendment or absorber of minerals in the soil, and therefore is produced under more controlled circumstances. The properties of biochar allow it to be a great absorber just like activated carbon, but also allow it to be a great facilitator of ion exchange. This allows it to better hold essential nutrients (such as NH_4^+) in the soil for plants to utilise. This is due to the large surface area of biochar, and increased charge density on the surface. Biochar is defined by European Biochar Certificate (EBC) as "a heterogeneous substance rich in aromatic carbon and minerals". Biochar is produced by biomass pyrolysis; a process whereby organic substances are broken down at temperatures ranging from 350 °C to 1000 °C in a low-oxygen thermal process. Torrefaction, hydrothermal carbonisation and coke production are further carbonisation processes whose end products cannot however be called biochar under the above definition. Biochars are therefore specific pyrolysis chars characterised by their additional environmentally sustainable production, quality and usage features. Gasification is understood as being part of the pyrolysis technology spectrum and can, if optimized for biochar production, be equally certified under the European Biochar Certificate (EBC) guidelines version 6.1).

Biochar is a material characterized by many environmental benefits:

Improvement of soil fertility [1] and crop yield [2];

Management and enhancement of agricultural products;

Reduction in CO_2 emissions into the atmosphere [3,4] thanks to the carbon sink process where carbon dioxide is subtracted from the cycle of carbon.

The DM 22 June 2015 update the D.L 75/2010 (all.2, 6, 7) relating to the reorganization and revision of regulations on fertilizers, published in GU 12 August 2015 [5] denotes the application of biochar as soil or substrate improver. Because the fine fraction of biochar (micrometrical size) is volatile and it could contain undesirable elements, the application of this substance in building materials or other composites is starting to gain more attention recently. Biochar has interesting properties for application in the building industry such as low thermal conductivity, high chemical stability and low flammability. Another characteristic of biochar is its capability to adsorb and desorb water, therefore materials containing biochar can be humidity control materials (HCM). The main requirement for this kind of material is good moisture absorption and desorption performance to detect and automatically adjust the relative air humidity. Various HCMs have been developed based on biomass, inorganic or organic raw materials. Specifically, in the literature, several studies have reported obtainment of HCMs using charcoal [6], diatomite [7], filled phos-

phates and aluminium oxide into the pores of sepiolite [8] as well as biochar-mortars [9]. Another application related to the high adsorption capacity of biochar reported in the literature is the adsorption and removal of pollutants in the aqueous phase on the surface of different kinds of geopolymers, both organics dyes and heavy metals [10]. The influence of various experimental factors such as geopolymer dosage, pH, initial dye concentration, contact time, and temperature was assessed for metakaolin geopolymers. The results demonstrated that the adsorption of the obtained material occurs spontaneously as an endothermic process, confirming that the prepared adsorbent can be used for remediation of water contaminated by methylene blue dye [11]. The activated FAs are demonstrated to be an efficient and low-cost adsorbent for decontamination of dye-containing water with the formation of new stable materials for encapsulation of aqueous solutions contaminated by high concentrations of methylene blue [12]. Biochar is also used to prepare a new biochar/geopolymer composite membrane by an in situ synchronous carbonation and self-activation process. The geopolymer membrane serves not only as a porous support, achieving good dispersion and retrieve of biochar, but also as a solid base for in situ activation of the biochar during carbonization of a lignin precursor [13].

There are also reports in the literature of the use of biochar in the construction field. In many applications, for example, cement or other building materials, an improvement of physical and thermal properties is found when biochar is added [14–17]. In the last year alone, interesting works have been published in this area which we report briefly below. In a mortar with silica fumes, the introduction of biochar reduces autogenic shrinkage and drying shrinkage and improves hydration, resistance and water permeability of the mortar [18]. In ultra-high performance concrete (UHPC) biochar as a mineral additive in partial replacement of cement, improves hydration thanks to its internal polymerization and nucleation effects [19]. Combined use of waste biochar and cement-based composites with CO_2 curing could be a green technology to improve cement properties (in particular mechanical strength) and carbon sequestration, together with promoting the recycling of waste [17]. The properties of biochar-cement composites depend on the lignocellulosic or non-lignocellulosic nature of the biomass from which the biochar is obtained, the former generally increasing the compressive strength, the elastic modulus and the fracture toughness [20]. Porous biochar, prepared from lignocellulosic biomass, improves the mechanical performance and durability of structural grade concrete and, in samples exposed to high temperatures, thermal damage is minimized and a good percentage of extra strength is maintained with respect to control concrete and silica fume [21]. Biochar has also been tested in lightweight aggregates (LWAs) for green roofs and bricks [22]. A very interesting class of materials both from a performance and environmental point of view, which researchers all over the world are looking at with attention, are geopolymers. They are characterised by low environmental impact, due to the raw materials used and the low-temperature processing, as well as by avoiding the use of carbonate-based raw materials, with corresponding CO_2 emissions, and expensive chemical reagents.

Geopolymers are inorganic materials with an amorphous or semi-crystalline nature consisting of a three-dimensional network of AlO_4 and SiO_4 tetrahedra. Geopolymerization is produced by a chemical reaction between a cementing component (source of aluminosilicates) and an alkaline activator, such as alkaline hydroxides and salts. For the synthesis of geopolymers, raw materials such as metakaolin, calcined clays, and industrial waste such as fly ash or slags have been used. In particular, when secondary raw materials such as fly ash or slag are used, due to their calcium content it is better to define the obtained material as alkali-activated material, and not as a geopolymer. Therefore, alkali-activated materials with optimized properties can be synthesized depending on many parameters, such as the selection of raw materials, process conditions and Si/Al ratio. According to Si to Al ratios, the repeated units of geopolymeric structures include poly-sialate (-Si-O-Al-), poly-sialate-siloxo (-Si-O-Al-O-Si-), poly-sialate-disiloxo (-Si-O-Al-O-Si-O-Si-) and sialate link [23]. Key characteristics of geopolymers make them potential environmentally friendly materials, namely, due to their sustainable fabrication method (exploitation of waste streams or by-

products and low energy consumption). The synergy between geopolymer industries and waste management is a significant boost to the development of geopolymer technologies providing a feasible pathway for the reduction of pollution and the valorisation of waste. Life cycle assessment studies demonstrate the eco-efficiency and low carbon footprint of this kind of waste-to-production stream [24,25].

In this paper, pre-treated incinerator bottom ash (IBA) and biochar are studied as geopolymers raw materials, in particular the valorisation of these residues is interesting because these materials can be produced anywhere in the world without territorial limitations. The first, which is an Italian commercial product, is an artificial inert aggregate based on aluminosilicates with a semicrystalline nature constituted by an amorphous fraction and many crystalline phases. It comes from a series of chemical-physical treatments of municipal solid waste incinerators bottom ash. The objective is minimizing waste production by transforming it into a reusable material, the so called "end of waste" (EOW). The treatment consists of ageing, sieving and washing. After the process, an inert material with silica-based matrix, rich in iron, calcium and aluminium oxides is obtained. This material can be successfully added in the formulation of cement or ceramic materials as substitute for mineral resources [26–31] and in geopolymers [32–34].

Other bottom ashes, different from incinerator ones, but rich in silica and alumina, have been successfully used in the geopolymer formulation, such as bottom ash from a thermal power plant [35], circulating fluidized bed combustion bottom ash [36–38], bagasse bottom ash [39], lignite bottom ash [40] and OXY-combustion and chemical looping combustion bottom ashes [41].

A novelty of this paper, is the use of a non-conventional aluminosilicate precursor in high percentages (up to 70 wt%) to obtain a porous material, without the addition of a foaming agent. In the literature, H_2O_2, metallic Al and Si have been used as foaming agents to produce geopolymeric foams with contents of biochar up to 30% [42,43]. Further, the present paper differs also from Farges et al., where biochar by-product-based geopolymer foams, using silica fume without metakaolin, were obtained [44].

Geopolymeric brick formation from exhausted paper mill sludge-derived biochar was also studied by Devi et al. [45].

In this context, the goal of this paper is to formulate lightweight chemically activated materials by using:

- non-hazardous biochar, which comes from gasification's process of woody biomasses from river maintenance,
- pre-treated bottom ash from urban incinerators, which acts as a foaming agent,
- metakaolin to optimize the Si/Al ratio in the mixture.

The advantage of adding biochar in the matrix is strictly related to its properties; it presents humidity exchange capacity, low density and high water adsorption that can be maintained in the final geopolymer.

2. Materials and Methods

2.1. Raw Materials

2.1.1. Raw Materials Characterization

The recovery raw materials are biochar and municipal incinerator bottom ash. The first originated from the gasification process of woody biomasses from maintenance operations of the Secchia river (Regional Project "REBAF") in a commercial gasification power plant, the All Power Labs PP20 (All Power Labs, 20187, Berkeley, CA, USA).

The second is a commercial product derived from the processing of municipal incinerator bottom ash (IBA) supplied by an authorized industrial plant located in Northern Italy. This product is mainly used as a partial replacement for natural raw materials, as a component of the meal fired in the cement plant kilns for the production of clinker and in concrete or asphalt as a replacement for natural sand or gravel. In this context, therefore, its use in geopolymeric materials can lead to higher added value products with improved properties related to the intrinsic characteristics of biochar.

The biochar was dried by heating at 105 °C in a muffle furnace for 24 h. Subsequently, it was ground and sieved to less than 250 µm. According to Vezzali et al. [22] the sieve analysis on biochar showed that 80.7% of the particle size distribution of biochar was less than 45 µm. The IBA, starting from course powder, was ground for 30 min in a ball mill and sieved below 75 µm. The goal of this process was to obtain grain size similar to the industrial metakaolin (MK) Argical 1000 supplied by BAL-Co, which has grains size <80 µm and is the principal component of geopolymers.

Chemical analysis was performed on metakaolin, IBA and biochar, which are the raw materials of alkali-activated materials, in order to identify the elements and their proportions (%). Chemical analysis of metakaolin was given by BAL-Co Spa. The IBA was analysed by X-ray fluorescence (Philips, PW2004) and its loss of ignition was performed at 1000 °C for 2 h. Chemical analysis of biochar was carried out with ICP analysis (ICP, Varian Liberty AX) with complete solubilization in acid in order to identify more precisely the inorganic elements in the material, and its loss of ignition was performed at 550 °C.

2.1.2. Mineralogical Analysis

Mineralogical analysis was performed in order to estimate the amorphous or crystalline nature of materials. X-ray diffraction analysis of IBA was carried out by a powder diffractometer (PW 3830, Philips, NL, USA) with Ni-filtered Cu Kα radiation in the 5–70° 2θ range on powdered samples. The determination of major crystalline phases of biochar was achieved by using an X-ray diffractometer on grounded and dried material (Philips, PW3710).

2.1.3. Physical Characterization

The physical characterization of biochar was performed by measuring the specific surface area, the absolute and apparent densities, and calculating the total porosity. Specific surface area was determined by the Brunauer–Emmett–Teller (BET) method (Micromeritics Gemini 2360): The biochar was outgassed for 24 h at 105 °C before measurement. The apparent density was estimated experimentally by adding a known quantity of biochar into a graduated cylinder to measure the volume and the biochar was dried in the oven at 105 °C before the analysis. The absolute density was measured by helium pycnometer (AccuPyc II 1340, Micromeritics, Norcross, GA, USA).

The BET analysis, apparent *Dapp* and absolute *Das* densities of the biochar were determined to evaluate the total porosity using Equation (1):

$$\mathrm{P_T}\% = \frac{Das - Dapp}{Das} * 100 \quad (1)$$

2.1.4. Biochar Absorption

A test has been provided in order to assess biochar's water absorption and release capacity. The test was carried out following the tea-bag method [46,47]: a tea filter, filled with about 5 g of biochar, was immerged in water, simultaneously a second empty filter was immersed in order to evaluate the amount of water absorbed by the biochar at different times.

$$\mathrm{Abs}\ \frac{g}{g}\mathrm{dried\ biochar} = \frac{Pf biochar' sachet - Pf\ empty\ sachet}{quantity\ biochar\ (5g)}$$

2.2. Geopolymers Preparation

Geopolymers were prepared by using metakaolin, biochar, IBA and two alkaline activator solutions, NaOH 8 M and Na_2SiO_3 (water glass).

The procedure for the samples' preparation was carried out according to the following steps.

(1) Mixing powders: The first composition was a mix of metakaolin and biochar and the second of metakaolin, IBA and biochar, both shed in a beaker in order to obtain a homogeneous mixture.

(2) Addition of sodium hydroxide solution (8 M) and sodium silicate solution (Si/Na = 3) (Rm = 3).
(3) Possible addition of few millilitres of water in order to obtain a liquid mixture. Water must be added if strictly necessary, otherwise it could slow down the subsequent hardening.
(4) Intensive shaking until a homogeneous and fluid paste was formed, in order to avoid formation of bubbles.
(5) Casting of the paste into a plastic mould.
(6) Closing of the mould inside a plastic bag for 24 h in order to avoid cracking and breakage.
(7) Maintaining the cast at room temperature.
(8) The curing phase at room temperature lasted 7 days, 30 days and 90 days.

In this study two different series of samples were prepared, both containing biochar, in order to estimate its possible interaction with the base matrix.

Because the biochar is very lightweight, it was added to metakaolin in volume percentages.

FIRST SERIES: metakaolin 100 wt%, and different percentages of biochar (20%, 30%, 40%, 50% and 70 vol%) were added to the base structure (Table 1 and Figure 2);

Table 1. Formulations of Series 1 and Series 2 samples (MK: Metakaolin; IBA: incinerator bottom ash; BC: Biochar in substitution).

SAMPLE	MK (g)	IBA (g)	BIOCHAR (vol%)	NaOH (mL)	Na_2SiO_3 (mL)	H_2O
MK100	50	\	\	24	34	\
MK + 20%biochar	50	\	(20%)	24	34	\
MK + 30%biochar	50	\	(30%)	24	34	\
MK + 40%biochar	50	\	(40%)	24	34	\
MK + 50%biochar	50	\	(50%)	24	34	\
MK + 70%biochar	50	\	(70%)	24	34	1
50MK-50IBA	25	25	\	8	20	\
50MK-50IBA + 20%biochar	25	25	(20%)	8	20	2
50MK-50IBA + 30%biochar	25	25	(30%)	8	20	5
50MK-50IBA + 40%biochar	25	25	(40%)	8	20	7
50MK-50IBA + 50%biochar	25	25	(50%)	8	20	9
50MK-50IBA + 70%biochar	25	25	(70%)	8	20	11
50MK-50BC	35.4	\	14.60 g	24	34	\

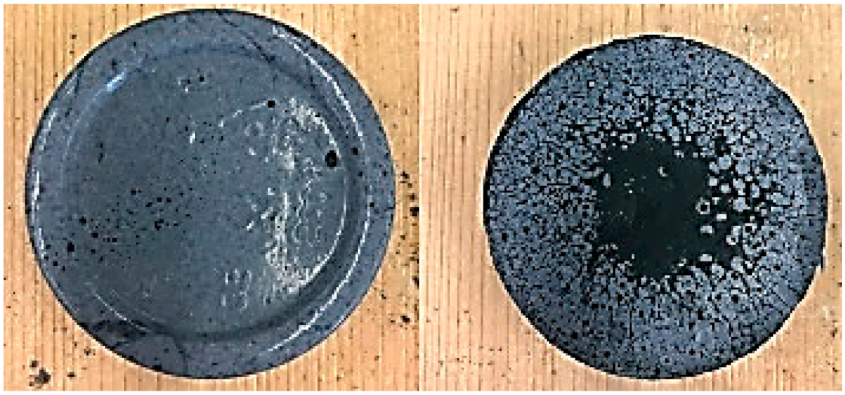

Figure 2. MK100 + 70%Biochar sample at 90 curing days.

The samples were compact with a smooth and porous surface. The surface showed efflorescence which created white stains. The efflorescence was a result of the migration of salts to the surface. The bottom ash (IBA) used in the study has high electrical conductivity values (0.7 mS/cm) due to the presence of chloride (340 mg/L) and sulphate (570 mg/L) anions and calcium (123 mg/L) and sodium (230 mg/L) ions. Efflorescence can also be generated from the reaction of excess of Na, deriving from the activating solutions, with atmospheric CO_2 forming Na_2CO_3, and can, therefore, be present in every geopolymer.

The efflorescence increased as the percentage of biochar increased because the effect of the biochar content on the efflorescence is related to the increase in porosity that permits the migration of salts contained in the IBA. The paste became less workable, and the activators could not reach all points of the material leading to non-homogeneous concentration of activating solutions and the corresponding efflorescence phenomenon.

SECOND SERIES: metakaolin, IBA (50/50 wt%) and different percentages of biochar (20%, 30%, 40%, 50% and 70 vol%) were added to the base matrix (Table 1 and Figure 3);

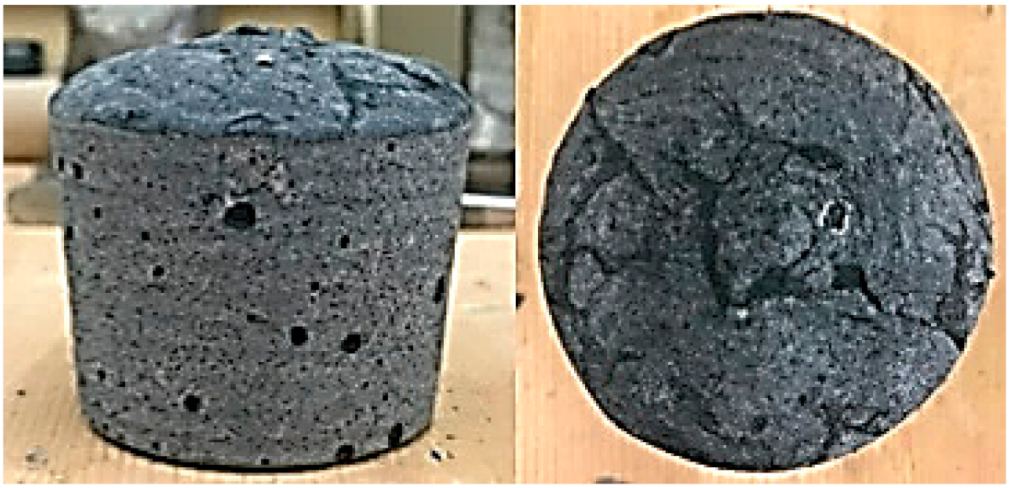

Figure 3. 50MK-50IBA + 70%Biochar at 90 curing days.

The samples swelled up due to the presence of IBA. The surface showed efflorescence which increased as the percentage of biochar increased, for the same reasons as in previous series.

Then a third composition was realized where biochar replaced 50% of the amount of metakaolin (50/50 vol%). This sample was characterized by 28 days of curing (Table 1).

2.3. Geopolymers Characterization

2.3.1. Integrity Test

The integrity test was carried out to evaluate the chemical resistance and the stability of the geopolymer. Three to four grams of the sample were immersed in distilled water for 24 h (solid/liquid ratio wt% was 1:100) at room temperature. The occurrence of the geopolymerization reaction was confirmed if the sample didn't dissolve in water.

2.3.2. Mineralogical Analysis

Mineralogical analysis was carried out in order to estimate if crystalline phases were developed during geopolymerization due to the presence of biochar and/or IBA. This test was performed by a powder diffractometer (PW 3710, Philips Research Laboratories, Netherlands) with Cu Kα radiation in the 5–70° 2θ range and speed of 1°/min, operating at 40 mA and 40 keV on powdered samples characterized by a grain size of 20–30 μm. Centre for Diffraction Data (ICCD) cards were used to identify the crystalline phases with the aid of XPert High Score software.

2.3.3. Chemical Stability

pH and ionic conductivity were measured to assess the geopolymerization process and three-dimensional reticulation of the geopolymer. The sample was broken and sieved below 250 μm in order to simulate the worst environment conditions for the material. Afterwards, each sample was tested in distilled water under stirring for 24 h in a beaker. pH (pH sensor Hamilton type Liq-glass SL) and conductivity (OAKTON Eutech Instruments CON 6/TDS 6) were measured after 5, 30, 60, 120, 240, 480, 1440 min.

2.3.4. Physical Characterization

Water absorption measures were conducted. The samples were dried, weighed and placed in distilled water for 24 h at room temperature. A difference in the samples between before and after immersion was noted:

$$\text{WA } (\%) = \frac{Pf - Pi}{Pi} * 100$$

The apparent (*Dapp*) (Enveloped Density Micromeritics Geopyc 1360) and absolute (*Das*) (Mycrometrics Accupyc 1340) densities provided quantitative information about the microstructure. From that assessment it was possible to determine the total porosity:

$$\text{P}_\text{T} \ (\%) = \frac{Das - Dapp}{Das} * 100$$

The BET (Brunauer–Emmett–Teller) analysis (Micromeritics Gemini 2360) allowed to determine the specific surface area of the alkali-activated materials. Generally, the BET method is performed on powder samples in order to evaluate the reaction degree during the sintering process. In this study the BET analysis was carried out on monolithic samples in order to evaluate the densification of the geopolymer samples, because the gas could enter the highly porous surface.

Hg intrusion porosimetry (Autopore IV9500, Micromeritics, Norcross, GA, USA) was carried out to measure pore size distribution, total pore volume, total pore surface area and sample densities (bulk and skeletal) which allowed us to evaluate open and closed porosity. The measures were conducted with an equilibrium time of 10 s, between pressure limits of 345 kPa and 228 MPa which enabled identification of capillary pores between 0.006 and 350 μm. These results were confirmed by ESEM (ESEM-QUANTA200, FEI Company, Hillsboro, OR, USA). Before SEM analysis the sample was coated with a Au-Pd sputtered layer.

2.3.5. Adsorption Capability of Alkali-Activated Materials

The behaviour of geopolymers in terms of water absorption from the environment was performed in two different ways. The first one was characterization in controlled temperature and humidity conditions, where the geo-polymeric sample was placed in a climatic chamber. In the second, the specimen was placed in variable temperature and humidity conditions in order to simulate the variation of climatic conditions over time. This case required information about maximum, minimum and average temperature and daily average relative humidity values for the observation period, which was provided by a weather station located in the department area.

3. Results

3.1. Raw Materials Characterization

Firstly, the raw materials were analysed in order to obtain their chemical analysis. In Table 2, chemical analyses of metakaolin, IBA, biochar and their loss of ignition (LOI) are shown. The biochar, despite its fine size, didn't form the geopolymeric matrix due to the content of Si and Al oxides not being high enough to form the aluminosilicate network. On the contrary, the IBA presented a SiO_2 + Al_2O_3 content of around 60% and therefore can

be defined an aluminosilicate precursor, able to form the aluminosilicate matrix typical of alkali-activated materials.

Table 2. Chemical analysis of MK, IBA, Biochar.

OXIDES (wt%)	MK	IBA	Biochar
SiO_2	58.97	53.90	26.10
Al_2O_3	34.70	5.67	2.42
Fe_2O_3	1.40	2.67	1.27
CaO	0.10	22.55	10.35
MgO	0.10	3.40	0.90
Na_2O	0.10	4.03	0.54
K_2O	0.70	0.94	2.57
TiO_2	1.30	1.55	0.02
LOI *	2.63	5.30	55.83

* (550 °C for biochar and 1000 °C for IBA).

3.1.1. Mineralogical Analysis

Mineralogical analysis was carried out in order to estimate the amorphous or crystalline nature of IBA and biochar. The XRD pattern of IBA is a typical amorphous/crystalline structure. The main phases are α-quartz (α-SiO_2), Calcite ($CaCO_3$), and aluminosilicates as Albite ($NaAlSi_3O_8$) and Gehlenite ($Ca_2Al(AlSi)O_7$), reflecting the chemical analysis of a typical ash rich in calcium and sodium (Figure 4). The whole characterization of IBA has been reported in the literature [27].

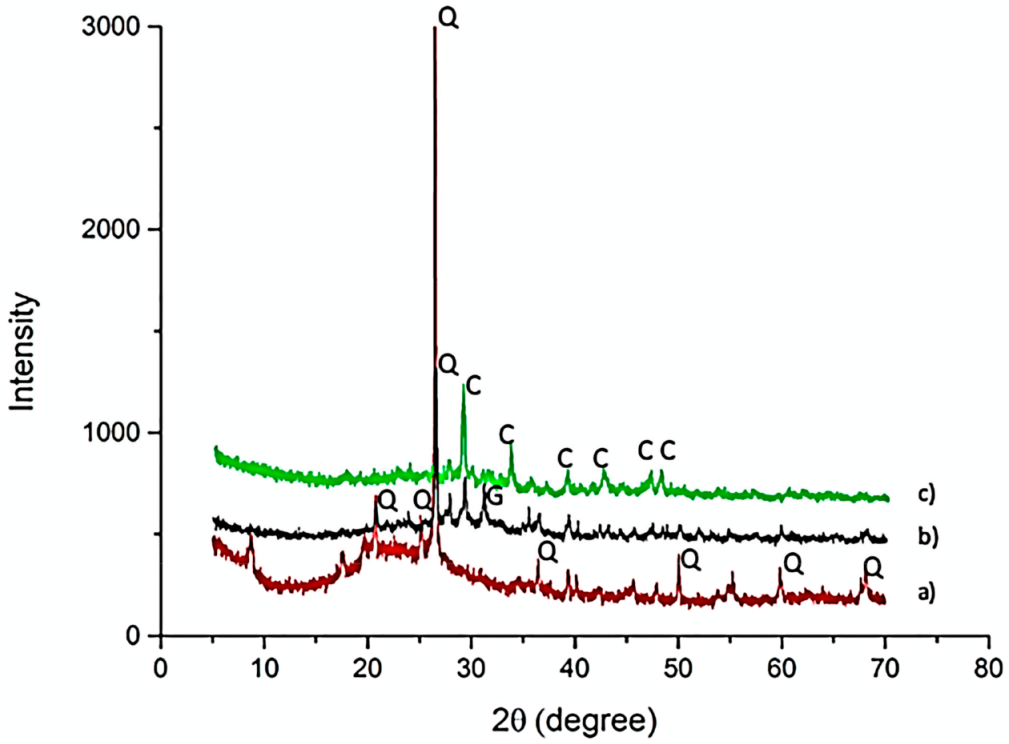

Figure 4. XRD patterns of raw materials: Metakaolin (a), IBA (b) and Biochar (c) (Q = Quartz; C = Calcite; G = Gehlenite).

Biochar is obtained at 900 °C, therefore its XRD pattern (Figure 4) shows a predominantly amorphous nature, visible as broad band in the 20–30 2θ range, corresponding to organic carbon, as reported in Vezzali et al. [22]. Indeed, the peak attributable to cellulose disappears when 400 °C is reached [48]. In this case, the only crystalline phases present can be identified mainly as Calcite ($CaCO_3$), with traces of Quartz (SiO_2), as observed in other studies [49].

3.1.2. Physical Characterization

The physical characterization of biochar (Table 3) shows that it was characterized by a high percentage, around 40%, of grains with diameter less than 100 µm. In accordance with the granulometric analysis, the biochar had a large specific surface area (210.50 ± 5.94 m^2 g^{-1}). The total porosity was estimated using Equation (1) from the apparent and absolute densities. According to Vezzali et al. [22], the bulk density was very low (0.16 g/cm^3) compared to other values in literature. Instead, the absolute density (2.23 g/cm^3) had a by higher value, because the biochar was derived by the gasification process at a high temperature. Increasing the processing temperature led to an increase in graphitization degree that produced an absolute density similar to that of solid graphite (2.25 g/cm^3) [22]. The total porosity obtained by the BET analysis was 92.8%, which is a high value and is similar to that found in other studies [50,51].

Table 3. BET, bulk density and total porosity results on biochar.

	Unity	Biochar
BET Surface Area	m^2 g^{-1}	210.50 ± 5.94
Apparent Density	g cm^{-3}	0.16
Absolute density	g cm^{-3}	2.23 ± 0.0004
Total Porosity	%	92.8

The teabag method provided realistic information about the amount of water that biochar absorbed and the available water that could be released from it at a later time [45]. The absorption occured in the first half an hour, while for longer times the weight remained almost constant, showing a saturation phenomenon; the same behaviour was observed in the cement pastes of Farzanian's research [45], where all the materials reached their equilibrium absorption during the measurement time. As showed in the Farzanian study, the high absorption of material could be attributed to its molecular structure, morphology and large surface area. Biochar was characterized by high capacity to absorb water, as showed by Figure 5, indeed it absorbed a quantity of water about six times its weight.

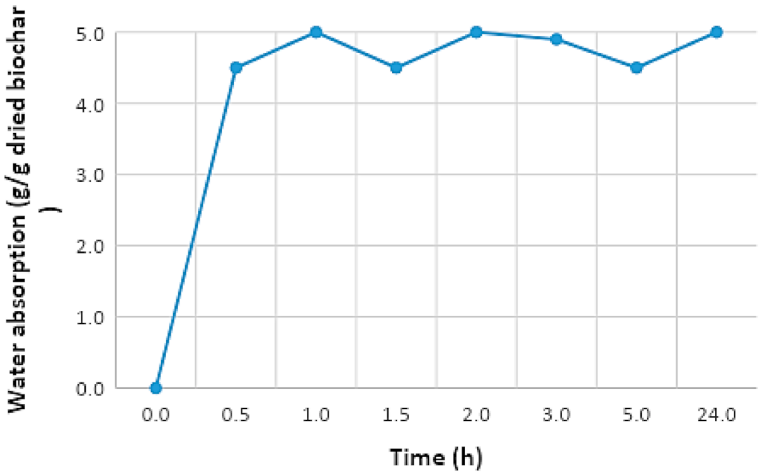

Figure 5. Water absorption trend of biochar.

3.2. Geopolymer Characterization

Geopolymers of the first and second series were characterized by curing times of 7, 28 and 90 days. Afterward curing, the samples were analysed.

3.2.1. Integrity Test

First, all samples (7, 28, 90 days of curing) were observed after 24 h of contact with water, in order to estimate the consolidation of the structure. None of the samples changed in appearance and water remained transparent without dispersed powder, confirming the occurrence of the geopolymerization reaction and the consolidation of samples. This integrity test has been adopted in our laboratory as a common procedure to demonstrate the chemical stability of alkali-activated materials containing complex aluminosilicate powders with variable chemical and mineralogical compositions, such as incinerator bottom ash [27] and mine tailings [52].

3.2.2. Mineralogical Analysis

Powder X-ray diffractometry analyses were performed in order to estimate the modification or formation of crystalline phases eventually induced by the geopolymerization phenomenon, as a consequence of the alkaline activation of metakaolin, biochar and IBA.

XRD patterns of the first set of samples (Metakaolin + Biochar) (Figure 6a) show no changes with the curing time. The patterns were characterized by two crystalline phases: at 2θ = 26.6°, quartz (SiO_2), which derives from metakaolin and at 2θ = 29.4°, calcite ($CaCO_3$), which derives from biochar. Indeed, calcite was evident only in the sample containing 70% of biochar. All the samples maintain the broad band typical of amorphous structures between 20–40° 2θ and a shift was observed with respect to the broad band characteristics of metakaolin, confirming geopolymerization. Samples of the third composition showed no mineralogical changes. The presence of quartz and calcite were observed because biochar was substituted for only 50% of the metakaolin.

XRD patterns of the second series samples (Metakaolin (MK) + IBA + Biochar) (Figure 6b) showed three principal peaks: at 2θ = 26.6°, quartz (SiO_2), due to metakaolin, at 2θ = 29.4°, calcite ($CaCO_3$), due to the biochar content, and at 2θ = 31°, gehlenite ($Ca_2Al(AlSi)O_7$), due to the IBA content. In general, the patterns of geopolymers presented an amorphous band at about 2θ = 25–35°, similar to other amorphous materials such as silicate glass. On the contrary, the broad band characteristic of amorphous carbon in biochar is located between 2θ = 15–25° and it is not visible in geopolymers. The patterns of the geopolymers (first and second series) showed no change as time of curing increased.

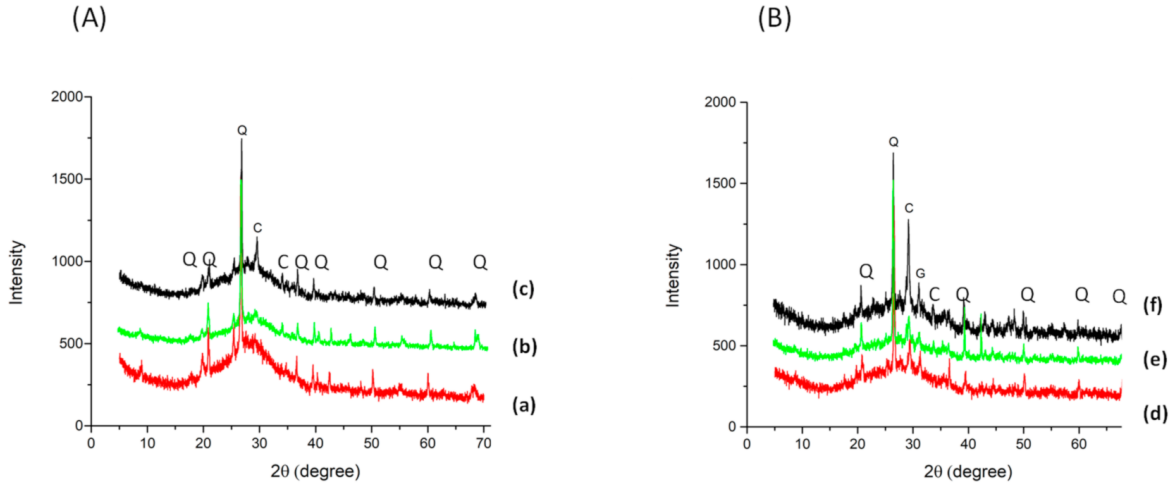

Figure 6. XRD patterns of (**A**) the first series: (a) MK100%, (b) MK + 20%Biochar and (c) MK + 70%Biochar and (**B**) the second series: (d) 50%MK/50%IBA, (e) 50%MK/50%IBA + 20%Biochar and (f) 50%MK/50%IBA + 70%Biochar (C = calcite; Q = quartz; G = gehlenite) at 90 days of curing.

3.2.3. Chemical Stability

In order to assess the geopolymerisation process and the three-dimensional reticulation, pH and ionic conductivity were determined at different times (5, 30, 60, 120, 240, 480, 1440 min) to evaluate the release of ions.

The first set of samples (Metakaolin + biochar) (Figure 7a) showed constant values of pH (from 10.5 to 11) as the biochar content increased, with no significant variations with respect to the geopolymer constituted by metakaolin only. The pH values were alkaline because of the natural alkaline nature of the geopolymers [27]. Moreover, the pH of alkali activators is very high, at around 14, but the geopolymers immersed in water develop a less alkaline pH due to the geopolymerization phenomenon because the activators (NaOH + Na-SiL) are not free, having reacted with the SiO_2 and Al_2O_3 available from the metakaolin.

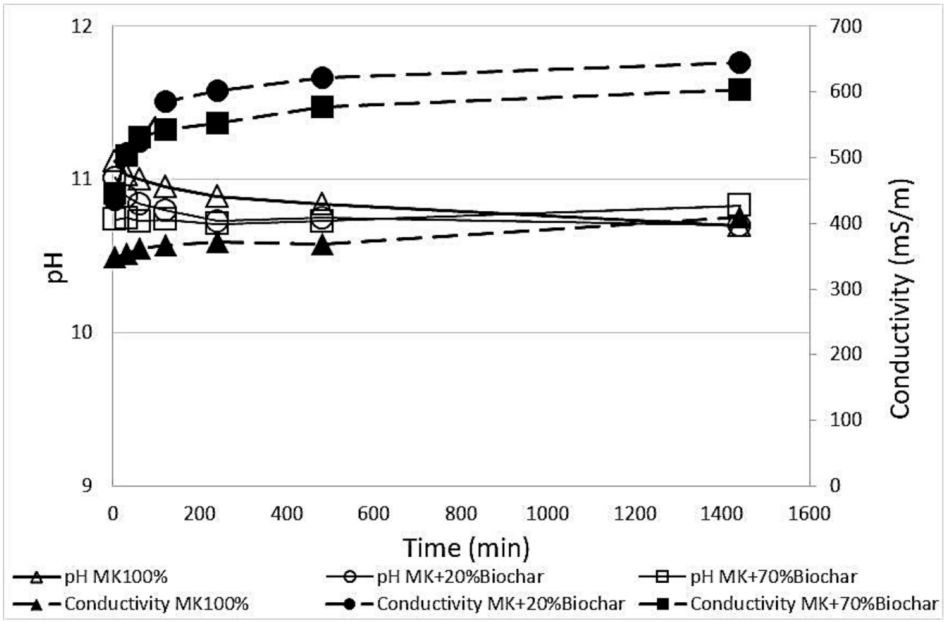

(**a**)

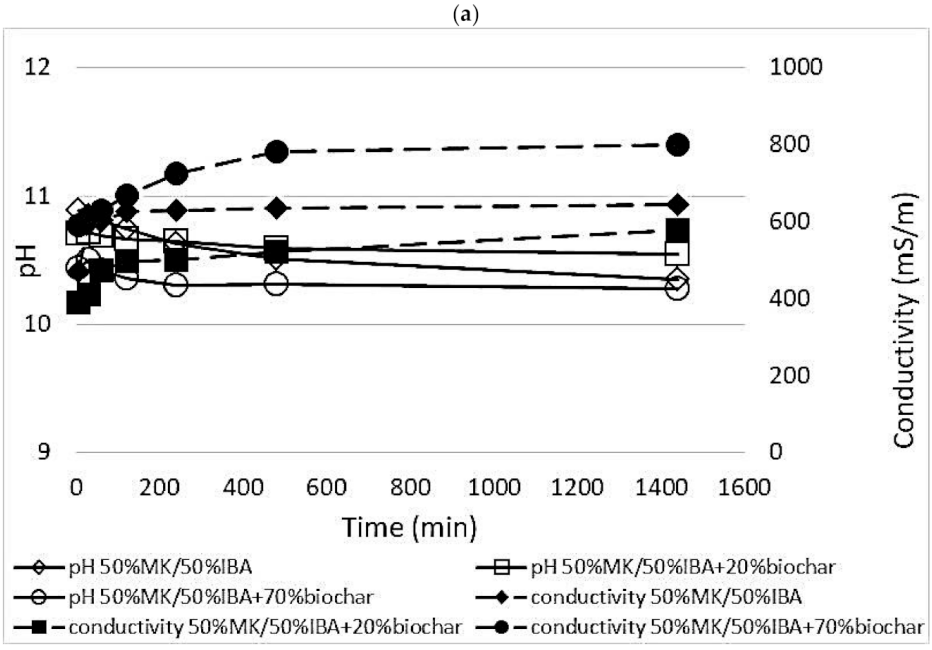

(**b**)

Figure 7. pH and conductivity trend of (**a**) first series samples and (**b**) second series samples at 90 days of curing.

Both the 28 and 90 (Figures 6a and 7a) days-of-curing samples were characterized by conductivity values which increased with added biochar (from 410 to 604 m Sm^{-1}). The chemical analysis of biochar shows the presence of Ca, and K, and the increase in conductivity is related to the release of these elements, indeed the pH characteristic of biochar is alkaline, as reported by Vezzali et al. [22].

This means that biochar didn't hinder the geopolymerization process which improved with time. Samples characterized by 90 days of curing were characterised by an increase in conductivity during the 24 h due to the number of ions released in the aqueous environment (from 445 to 604 m Sm^{-1} for the sample with metakaolin and 70% biochar). An important aspect is the trend of conductivity depending on curing time. The increase in curing time involved a higher stability material and a higher geopolymerization degree confirmed by a reduction in released ions in the solution. This meant that the conductivity values decreased from 785 to 604 m Sm^{-1}, for example, for the same sample with metakaolin and 70% of biochar at 28 and 90 curing days.

The second series samples (Metakaolin + IBA + biochar) (Figure 7b) confirmed the results of the first series, showing constant values of pH around 10.5–11.0. The ionic conductivity increased as the percentage of biochar increased (from 646 to 801 m Sm^{-1}) for the sample with 90 days of maturation, due to the saline content of biochar and IBA. For example, the sample containing 20% of biochar had a conductivity value around 500 m Sm^{-1} while the sample with 70% of biochar content had a value around 700 m Sm^{-1}. This means that the samples with higher percentage of biochar, for example 70%, showed higher release of ions in solution due to their microstructure and ions released related to the biochar.

The ionic conductivity of the second series samples showed higher values than samples of the first series (from 604 to 801 m Sm^{-1}) because the interaction with the external environment was higher and the presence of IBA in the formulation led to less stability and compactness of the material.

The third series' composition was characterized by constant values of pH around 11 and conductivity around 800 m Sm^{-1}.

3.2.4. Physical Analysis

Microstructural observations defined that samples of the first series (Metakaolin (MK) + biochar) were characterized by a specific surface which increased as the percentage of biochar increased, as shown by BET analysis (Table 4). BET analysis shows an increase in specific surface with increasing biochar content, which is a porous material.

Table 4. BET of MK100%, MK + 50%Biochar and MK + 70%Biochar samples at 90 curing days.

SAMPLE	BET (m^2 g^{-1})
MK100	23.81 ± 0.1848
MK + 50%Biochar	39.21 ± 0.3538
MK + 70%Biochar	46.45 ± 0.7282

Samples containing metakaolin and metakaolin + biochar were characterized by high open porosity. When biochar was introduced into the geopolymers, open porosity reduced: the sample with 100% metakaolin without biochar showed open porosity around 47%, while the sample containing 70% biochar had 42%. This result was due to biochar acting as a filler going into the pores, while the biochar itself is porous. The high values of open porosity were confirmed by measurements of apparent density and high values of water absorption. Apparent density remained constant as the percentage of biochar increased because the biochar influenced only the open porosity.

The sample characterized by 70% biochar showed a decrease in open porosity but a high value of water absorption due to the significant capability of biochar to adsorb water (about six times its weight), according to Farzanian [45], where the absorption capacity of

cement pastes was reported. Similar findings can be found from other authors [14], with the addition of pyrolyzed agro-food biochar to magnesium phosphate cement. They show that biochar causes a decrease in porosity, confirming the filler effect.

Figure 8 shows the same behaviour of all the geopolymers independently of the proportion of biochar, with an increase in water absorption for longer curing times. Furthermore, increasing the biochar content increases the extent of the phenomenon going from 46% for the MK100 geopolymer to 77% for the 70% of biochar geopolymer. This behaviour occurs because biochar is characterized by high absorbtion capacity (biochar can adsorb a quantity of water about six times its weight).

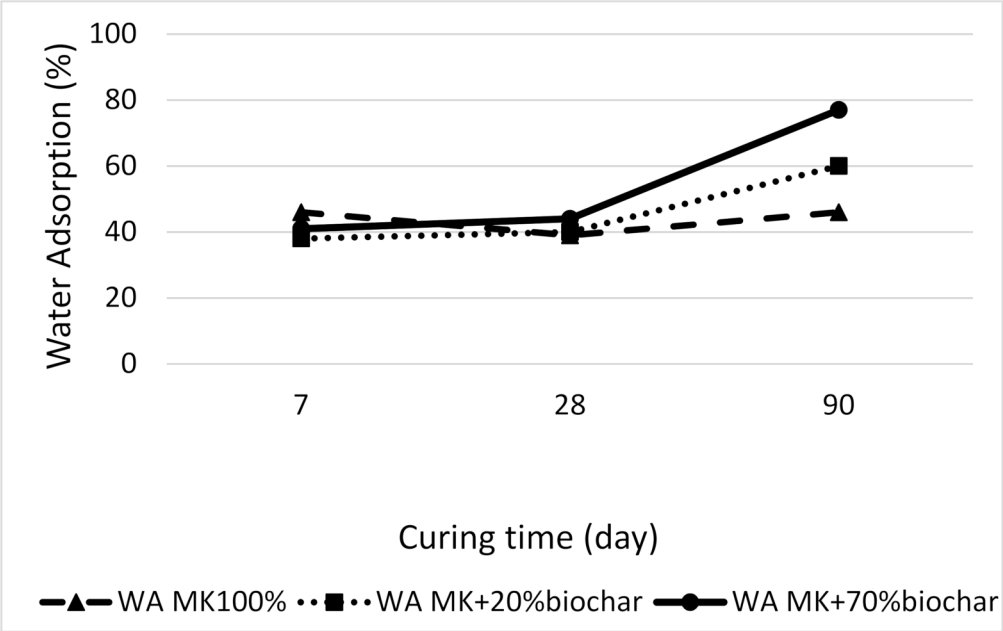

Figure 8. WA trend of MK + Biochar series at 7, 28, 90 days of curing.

From intrusion porosimetry analysis it is possible to follow the evolution of the curing process of the prepared geopolymers. The data reported in Table 5 show the decrease in total Hg intrusion volume, pore area and total porosity when comparing 28- and 90-day specimens without biochar due to the geopolymerization. On the other hand, specimens containing 70% biochar after 28 and 90 days showed an increase in total Hg intrusion volume, pore area and total porosity but a decrease in the dimensions of pores. This characteristic derives from the presence of biochar which is itself a porous material and also fills the open pores, reducing the dimensions. The effect of the biochar addition (20, 70 vol%) on the geopolymer microstructure is displayed in Figure 9 for samples after 90 days of curing. It is possible to note for all specimens analysed, the sigmoidal trend indicating spherical pore shape [53]. The cumulative intrusion curves are overlapped until the region where majority of pores are present for these materials in the range (6–100 nm). The plots show an increase in the total Hg volume intruded, synonymous with total pore volume, when the amount of biochar present in the composition increased. These results indicate that the presence of biochar plays a crucial role in the pore formation (dimensions, pore area and total volume) in the structure.

Another interesting findings regarding the role played by biochar when added as filler or in substitution of metakaolin is reported in Table 5. The specimen containing 50% biochar as filler showed a lower total porosity with respect to those in substitution which display high pore volume, area and dimensions of pores. This behaviour of samples with biochar replacing metakaolin is related to the lesser amount of metakaolin, which is responsible for the consolidation process. Farges et al., also demonstrated the possibility to successfully synthesize geopolymers based on 60 wt% metakaolin and 40 wt% biochar [44].

Calculating open and closed porosity from the densities, it emerged that the presence of biochar in substitution for metakaolin caused an absence of closed porosity (from 1.99% to 0.08%) in the microstructure and only open porosity was formed. The results are in agreement with the WA% and SEM analysis, reported below. Tan et al. [10] reported that in a porous geopolymer obtained by direct foaming methods with hydrogen peroxide, H_2O_2 and metallic Al or Si powders, the pore sizes usually ranged from nanometres up to millimetres with total pore volume ranging from 30 to 90%, which is in line with the findings of this work.

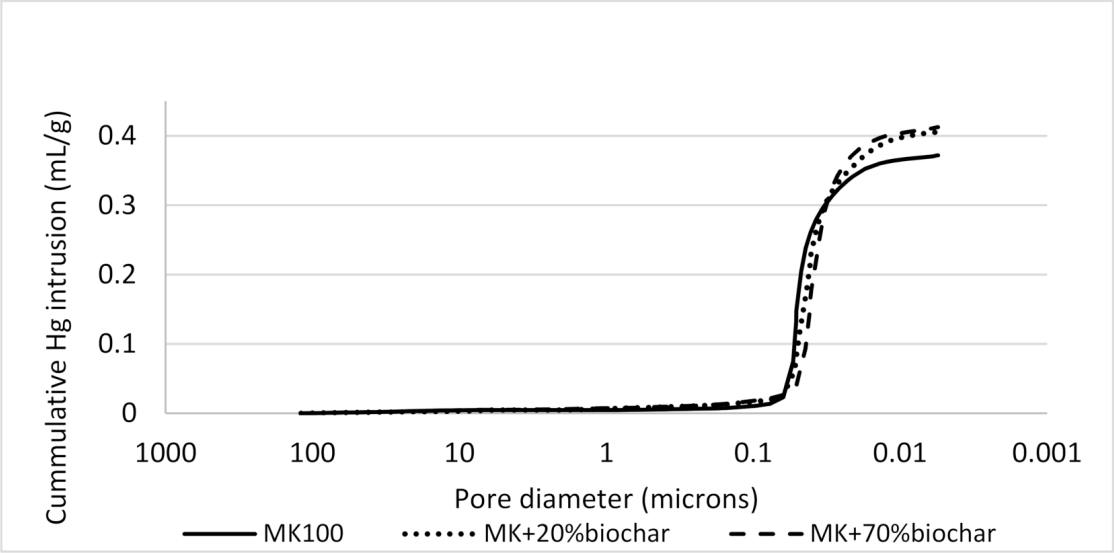

Figure 9. Cumulative intrusion curves for samples containing 0–20 and 70 vol% of biochar after 90 days of curing.

Table 5. MIP parameters determined for the different compositions (MK: metakaolin; B: biochar).

Sample	Total Intrusion Hg Volume ($m^3\ g^{-1}$)	Total Pore Area ($m^2\ g^{-1}$)	Average Pore Diameter (μm)	Total Porosity (%)
MK100 28 d	$399.5 \times 10^{-6} \pm 1 \times 10^{-6}$	41.552	0.0385 ± 0.0001	45.2198
MK100 90 d	$371.9 \times 10^{-6} \pm 1 \times 10^{-6}$	39.841	0.0373 ± 0.0001	43.9117
MK + 20%biochar 90 d	$406.2 \times 10^{-6} \pm 1 \times 10^{-6}$	49.290	0.0330 ± 0.00015	45.4361
MK + 70%biochar 90 d	$412.5 \times 10^{-6} \pm 1 \times 10^{-6}$	51.127	0.0323 ± 0.0001	46.1124
50MK-50BC 28 d	$459.5 \times 10^{-6} \pm 1 \times 10^{-6}$	58.196	0.0316 ± 0.0001	49.7563
MK + 50%biochar 28 d	$371.6 \times 10^{-6} \pm 1 \times 10^{-6}$	53.040	0.0280 ± 0.00007	43.9968

3.2.5. Microstructural Analysis

SEM analysis confirmed the previous observations. In fact, the surface of the sample without biochar was characterized by smooth and compact aspect with isolated pores (Figure 10a). When the biochar was added to the matrix, the surface became porous, with tubular and hive structures typical of the biochar nature (see white marked area) (Figure 10b). Morphological characterization reported by other authors shows uneven ridges on the surface typical of biochar derived from woody biomass [18,21]. However, as the percentage of biochar inside the matrix increased, the surface presented less porosity because biochar filled the pores: a compact and resistant material was obtained.

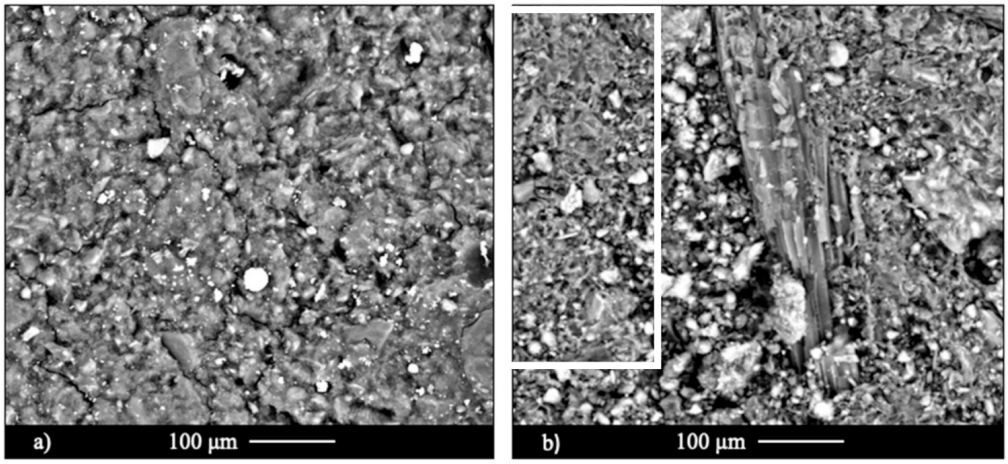

Figure 10. Internal surface (**a**) of MK 100%; Internal surface (**b**) of MK + 70%biochar.

When biochar replaced metakaolin, and was not added to it (series 3), total porosity increased (Figure 11). The open porosity increased because there was a higher content of biochar with respect to metakaolin responsible for densification. The increase in open porosity was confirmed by water absorption values. In fact, when biochar was added to metakaolin the value was around 36%, while when biochar replaced metakaolin, the absorption value was 54%.

Sample characterization showed that samples of the second set containing aluminosilicate precursor (Metakaolin + IBA + Biochar) as the matrix, with 90 days of curing, were characterized by reduction in apparent density as the percentage of biochar increased. Biochar was inserted into matrix's pores and consequently produced a lightweight and porous material.

The WA% values increased for several reasons, first, due to biochar content, with biochar being a lightweight material with high water absorption capacity and the microstructural properties of IBA.

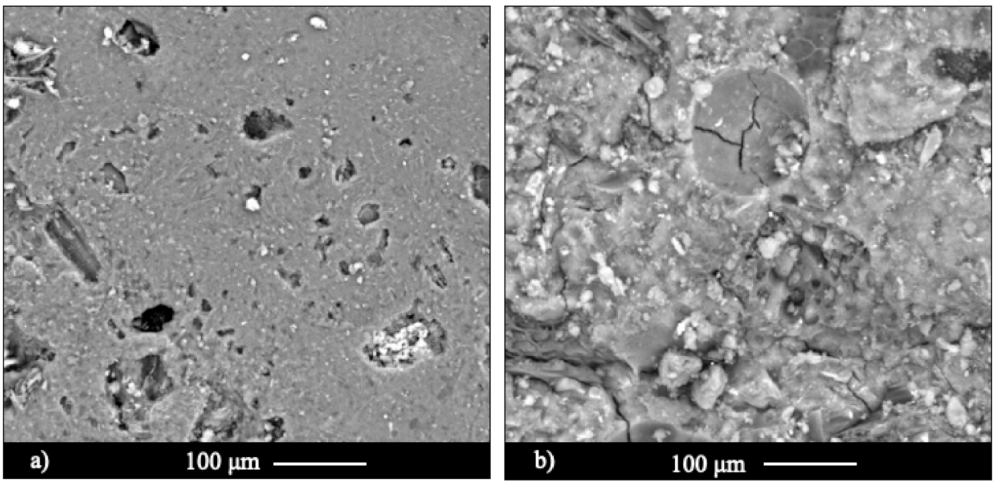

Figure 11. External (**a**) and internal (**b**) surface of SERIES 3 where MK is replaced by biochar.

The trend in Figure 12 is different with respect to the set without a matrix. The addition of 20% of biochar leads to a decrease in WA because biochar particles can fill the porosity due to IBA. This behaviour was observed by other authors [19,21] who also attribute the reduction in water absorption to the filler effect of biochar particles due to its finer particle size, and internal curing effect contributing to hydration and pore filling. Otherwise for higher additions of of biochar (70%) the lightweight characteristic and the adsorption capability of biochar leads to an increase in water absorption of geopolymers.

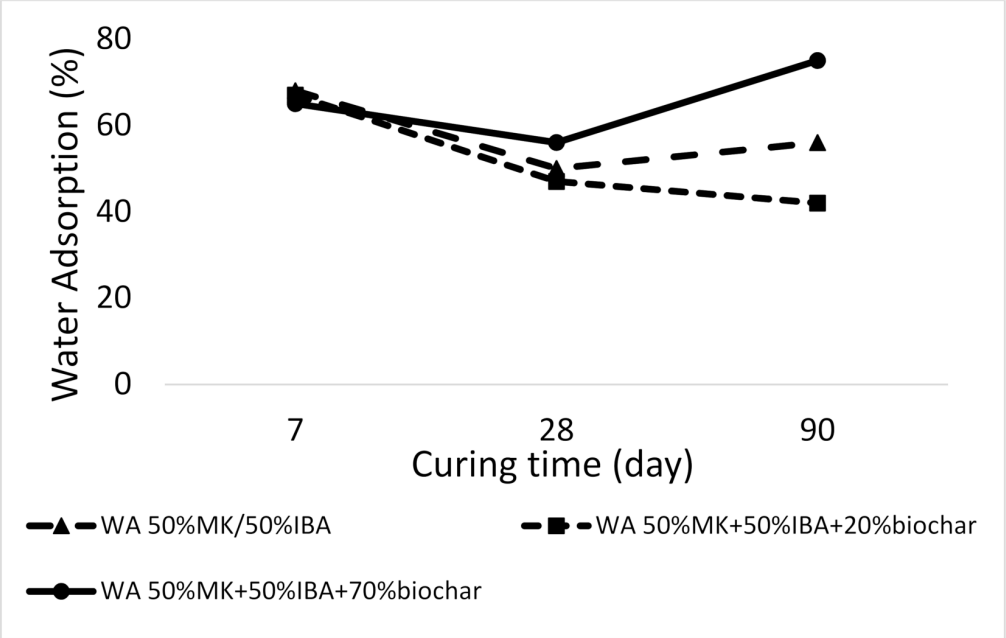

Figure 12. WA trend of 50% MK-50% IBA + Biochar at 7, 28, 90 days of curing.

SEM analysis showed high porosity in the sample without biochar (only MK + IBA) (Figure 13a) compared to the MK100 sample due to the reactivity of Al contained in the IBA which, in the alkaline environment typical of geopolymers, leads to the formation of H2 gas. This gas causes the formation of pores in the matrix. Even in this series, biochar filled porosity, producing a compact structure yet able to maintain the lightness. SEM images were confirmed by high values of BET, which showed structured and dense material (Tables 4 and 6).

Table 6. BET of 50% MK-50% IBA with the addition of 50 or 70% of biochar at 28 curing days.

SAMPLE	BET (m^2 g^{-1})
50% MK-50% IBA	19.42 ± 0.1773
50% MK-50% IBA + 50%biochar	30.43 ± 0.3201
50% MK-50% IBA + 70%biochar	38.72 ± 0.6309

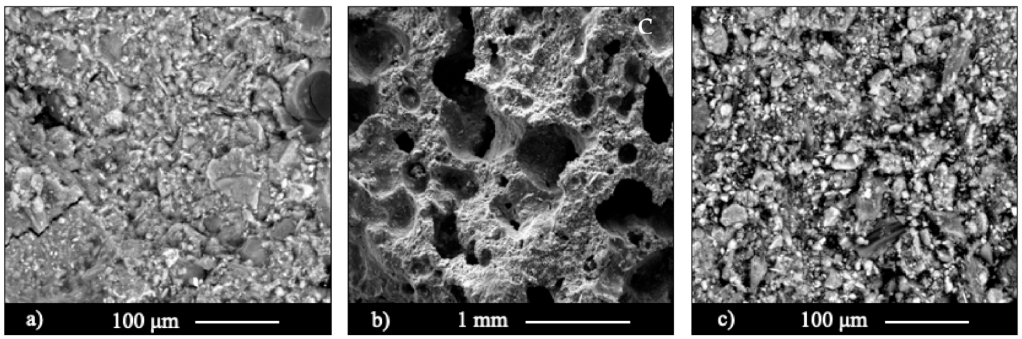

Figure 13. Internal surface of 50% MK-50% IBA (**a**), and (**b**) and 50% MK-50% IBA + 70%Biochar (**c**).

3.2.6. Absorption of Alkali-Activated Materials Results

Biochar had a strong adsorbent capacity, so another aspect studied was the adsorption and release of moisture (Figure 14). The test was carried out in controlled and variable conditions of temperature and humidity.

The first context simulated in a climatic chamber an indoor environment (T = 20 °C, humidity = 50%). The samples of the first series, containing MK where biochar was added, absorbed and released more moisture as the percentage of biochar increased, because biochar had a strong absorbent capacity.

The second context simulated an outdoor environment (temperature and humidity data were provided by the weather station of the department). The test showed a progressive increase in weight as a function of humidity.

In the first context, the second series samples containing IBA were characterized by greater capacity of absorption and release of humidity. This result was obtained from the synergistic effect of biochar's properties and intrinsic characteristics of IBA. In the second context samples showed a correlation between the changes in humidity of materials and the water content. In both compositions there was a delay in the mechanism of absorption of moisture due to (a) positioning of the sample in the atrium, which is not a completely an external environment, but simulates one, and (b) the diffusive motion of the molecules of gaseous water within the open porosities is not immediate. This behaviour can enhance the regulatory effect on the environmental humidity. Wang et al. [17] found that the addition of biochar improved cement hydration, which was attributed to moisture regulation effect. This conclusion can be related to biochar's capacity to hold water in its porous structure, gradually releasing it for hydration. Additionally the initial decrease in water absorption shown in Figure 12, when biochar was added to the MK/IBA series, can be related to the water content of biochar.

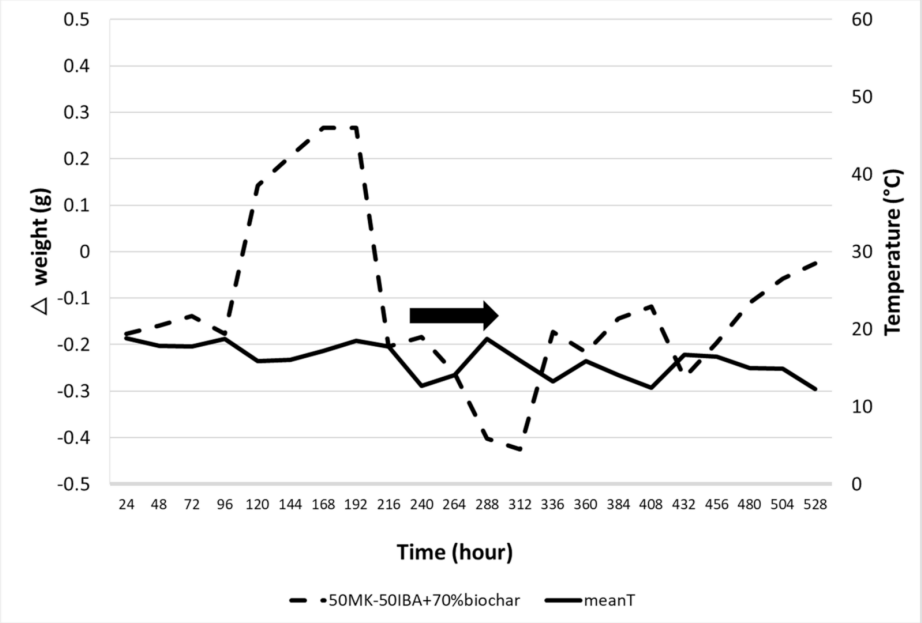

Figure 14. Absorption and release of humidity of MK + 70%biochar samples in an outdoor environment and 50% MK_50% IBA + 70%biochar samples in an outdoor environment.

To conclude, analysing all the obtained results, it can be observed that the properties of biochar were maintained in the prepared geopolymers. In particular, lightness, water absorption and humidity exchange capacity. All these characteristics are related to nature of biochar which has high absorption capacity corresponding to six times its weight, according to literature values. This capacity also influences the water absorption, which is high, notwithstanding that addition of biochar leads to a decrease in porosity (from 47% for metakaolin and 42% for biochar geopolymer), because it plays the role of filler in the matrix, as was observed in the SEM images. The effect of IBA without biochar was both high porosity and high water absorption and the filler effect of biochar was more evident in this series than in the metakaolin one.

4. Conclusions

The aim of this research was to evaluate the possibility of realizing lightweight alkali-activated materials exploiting biochar. Biochar is a secondary raw material coming from pyrolysis/gasification processes with some environmental benefits, such as (i) improvement of soil fertility, (ii) reduction of CO_2 emissions into the atmosphere thanks to the carbon sink process where carbon dioxide is subtracted from the cycle of carbon.

For the matrix of geopolymers an end-of-waste material, derived from incinerator bottom ash, was used and compared to pure metakaolin matrix. The introduction of an alternative aluminosilicate precursor in geopolymers could lead to a reduction in the consumption of natural resources, sustainable waste management and energy recovery. Further, the chemical characteristics of this precursor result in a porous material without the addition of a foaming agent.

The possibility to obtain geopolymers was confirmed by the results, and no hindering of geopolymerization was observed due to the presence of biochar and/or incinerator bottom ash. The materials obtained are lightweight and porous, with high water absorption capacity and moisture adsorption/desorption. As a future perspective, different types of biochar should be compared to each other. Farges et al. [44] show that physicochemical and structural characteristics depend on the nature and the chemical composition of the starting biomass, and on the pyrolysis temperature. These parameters lead to different chemical biochar compositions with corresponding different reactivity.

Nowadays, biochar is used as amendment in soils, but the finer fraction can cause problems of dispersion in the environment due to their lightness and physical volatility. The massive spreading of biochar in the soil could lead to significant environmental consequences. The biochar fraction used was less than 250 μm but the real grain size exploited in this work was 45 μm, so this fraction can be exploited in geopolymers where the low particle size is an advantage because it leads to higher reactivity. Powders such as PM2.5 and PM10 cause environmental dispersion and monitoring problems. Due to the intrinsic characteristics of the biochar, such as lightness this effect is found also for larger grain sizes, so their use as an additive in building materials rather than dispersing in the environment could be an interesting solution.

Due to the technical properties of materials containing biochar they can be used in the future for a cleaner design of products in the field of sustainable construction for insulating panels or lightweight materials for house and garden in terraces and balconies.

Author Contributions: F.P., measurements and lab activity; F.A., coordination of lab activity; L.B. and I.L., supervisor. All authors have read and agreed to the published version of the manuscript.

Funding: Research was supported by regional project POR-FESR REBAF (2016–2018), (PG/2015/854163).

Data Availability Statement: Not applicable.

Acknowledgments: Authors thank Emilia Romagna Region, project POR-FESR REBAF (2016–2018), (PG/2015/854163).

Conflicts of Interest: The authors declare that they have no conflict of interest.

References

1. Van Zwieten, L.; Kimber, S.; Sinclair, K.; Chan, K.Y.; Downie, A. Biochar: Potential for Climate Change Mitigation, Improved Yield and Soil Health. In Proceedings of the 23rd Annual Conference of the Grassland Society of NSW 152, Tamworth, UK, 21–23 July 2008; Available online: http://grasslandnsw.com.au/news/wp-content/uploads/2009/07/Van-Zweiten-Kimber-Sinclair-Chan-Downie-2008.pdf (accessed on 10 November 2021).
2. Yamato, M.; Okimori, Y.; Wibowo, I.F.; Anshori, S.; Ogawa, M. Effects of the application of charred bark of Acacia mangium on the yield of maize, cowpea and peanut, and soil chemical properties in South Sumatra, Indonesia. *Soil Sci. Plant Nutr.* **2006**, *52*, 489–495. [CrossRef]
3. Glaser, B.; Lehmann, J.; Zech, W. Ameliorating physical and chemical properties of highly weathered soils in the tropics with charcoal—A review. *Biol. Fertil. Soils* **2002**, *35*, 219–230. [CrossRef]
4. Lehmann, J. Bio-energy in the black. *Front. Ecol. Environ.* **2007**, *5*, 381–387. [CrossRef]

5. Italian Law DM 22/06/2015 Updated by D.L 75/2010 (all.2,6,7) relative to the reorganization and revision of regulations on fertilizers published in GU 12/08/2015.
6. Hasegawa, T.; Iwasaki, S.; Shibutani, Y.; Abe, I. Preparation of superior humidity-control materials from kenaf. *J. Porous Mater* **2009**, *16*, 129–134. [CrossRef]
7. Zheng, J.; Shi, J.; Ma, Q.; Dai, X.; Chen, Z. Experimental study on humidity control performance of diatomite-based building materials. *Appl. Therm. Eng.* **2017**, *114*, 450–456. [CrossRef]
8. Ding, Y.; Meng, J.; Liang, J.; Li, G.; Liang, X. Preparation and their property of porous mineral ecomaterials for ambient humidity self-controlling. *Xiyou Jinshu Cailiao Yu Gongcheng/Rare Met. Mater. Eng.* **2004**, *33* (Suppl. S2), 114–118.
9. Park, J.H.; Kim, Y.U.; Jeon, J.; Yun, B.Y.; Kang, Y.; Kim, S. Analysis of biochar-mortar composite as a humidity control material to improve the building energy and hygrothermal performance. *Sci. Total Environ.* **2021**, *775*, 145552. [CrossRef]
10. Tan, T.H.; Mo, K.H.; Ling, T.C.; Lai, S.H. Current development of geopolymer as alternative adsorbent for heavy metal removal. *Environ. Technol. Innov.* **2020**, *18*, 100684. [CrossRef]
11. El Alouani, M.; Alehyen, S.; El Achouri, M. Preparation, Characterization, and Application of Metakaolin-Based Geopolymer for Removal of Methylene Blue from Aqueous Solution. *J. Chem.* **2019**, *2019*, 4212901. [CrossRef]
12. El Alouani, M.; Alehyen, S.; El Achouri, M.; Taibi, M. Comparative study of the adsorption of micropollutant contained in aqueous phase using coal fly ash and activated coal fly ash: Kinetic and isotherm studi. *Chem. Data Collect.* **2019**, *23*, 100265. [CrossRef]
13. Huang, J.; Li, Z.; Zhang, J.; Zhang, Y.; Ge, Y.; Cui, X. In-situ synchronous carbonation and self-activation of biochar/geopolymer composite membrane: Enhanced catalyst for oxidative degradation of tetracycline. *Chem. Eng.* **2020**, *397*, 125528. [CrossRef]
14. Ahmad, M.R.; Chen, B.; Duan, H. Improvement effect of pyrolyzed agro-food biochar on the properties of magnesium phosphate cement. *Sci. Total Environ.* **2020**, *718*, 137422. [CrossRef] [PubMed]
15. Sirico, A.; Bernardi, P.; Belletti, B.; Malcevschi, A.; Dalcanale, E.; Domenichelli, I.; Fornoni, P.; Moretti, E. Mechanical characterization of cement-based materials containing biochar from gasification. *Constr. Build. Mater.* **2020**, *246*, 118490. [CrossRef]
16. Yang, S.; Wi, S.; Lee, J.; Lee, H.; Kim, S. Biochar-red clay composites for energy efficiency as eco-friendly building materials: Thermal and mechanical performance. *J. Haz. Mater.* **2019**, *373*, 844–855. [CrossRef]
17. Wang, L.; Chen, L.; Tsang, D.C.W.; Guo, B.; Yang, J.; Shen, Z.; Hou, D.; Ok, Y.S.; Poon, C.S. Biochar as green additives in cement-based composites with carbon dioxide curing. *J. Clean. Prod.* **2020**, *258*, 120678. [CrossRef]
18. Gupta, S.; Krishnan, P.; Kashani, A.; Kua, H.W. Application of biochar from coconut and wood waste to reduce shrinkage and improve physical properties of silica fume-cement mortar. *Constr. Buid. Mater.* **2020**, *262*, 120688. [CrossRef]
19. Dixit, A.; Gupta, S.; Dai Pang, S.; Kua, H.W. Waste Valorisation using biochar for cement replacement and internal curing in ultra-high performance concrete. *J. Clean. Prod.* **2019**, *238*, 117876. [CrossRef]
20. Gupta, S.; Palansooriya, K.N.; Dissanayake, P.D.; Ok, Y.S.; Kua, H.W. Carbonaceous inserts from lignocellulosic and non-lignocellulosic sources in cement mortar: Preparation conditions and its effect on hydration kinetics and physical properties. *Constr. Build. Mater.* **2020**, *264*, 120214. [CrossRef]
21. Gupta, S.; Wei, K.H.; Dai, P.S. Effect of biochar on mechanical and permeability properties of concrete exposed to elevated temperature. *Constr. Build. Mater.* **2020**, *234*, 11733. [CrossRef]
22. Vezzali, V.; Andreola, F.; Barbieri, L.; Lancellotti, I.; Pozzi, P.; Allesina, G.; Pedrazzi, S.; Tartarini, P. Gasification of biomass from river maintenance and char application in building materials production. *Env. Eng. Manag. J.* **2018**, *17*, 2485–2496. [CrossRef]
23. Joseph, D. Properties of geopolymer cements. In Proceedings of the 1st International Conference on Alkaline Cements and Concretes, Kiev, Ukraine, 24–26 June 1994; pp. 131–149.
24. Blengini, G.A.; Busto, M.; Fantoni, M.; Fino, D. Eco-efficient waste glass recycling: Integrated waste management and green product development through LCA. *Waste Manag.* **2012**, *32*, 1000–1008. [CrossRef]
25. Jiang, M.; Chen, X.; Rajabipour, F.; Hendrickson, C.T. Comparative life cycle assessment of conventional, glass powder, and alkali-activated slag concrete and mortar. *J. Infrastruct. Syst.* **2014**, *20*, 04014020. [CrossRef]
26. Ferraris, M.; Salvo, M.; Ventrella, A.; Buzzi, L.; Veglia, M. Use of vitrified MSWI bottom ashes for concrete production. *Waste Manag.* **2009**, *29*, 1041–1047. [CrossRef]
27. Lancellotti, I.; Ponzoni, C.; Barbieri, L.; Leonelli, C. Alkali activation process for incinerator residue management. *Waste Manag.* **2013**, *33*, 1740–1749. [CrossRef]
28. Lancellotti, I.; Ponzoni, C.; Bignozzi, M.C.; Barbieri, L.; Leonelli, C. Incinerator bottom ash and ladle slag for geopolymers preparation. *Waste Biomass Valorization* **2014**, *5*, 393–401. [CrossRef]
29. Rambaldi, E.; Esposito, L.; Andreola, F.; Barbieri, L.; Lancellotti, I.; Vassura, I. The recycling of MSWI bottom ash in silicate based ceramic. *Ceram. Int.* **2010**, *36*, 2469–2476. [CrossRef]
30. Schabbach, L.M.; Andreola, F.; Lancellotti, I.; Barbieri, L. Minimization of Pb content in a ceramic glaze by reformulation the composition with secondary raw materials. *Ceram. Int.* **2011**, *37*, 1367–1375. [CrossRef]
31. Schabbach, L.M.; Andreola, F.; Barbieri, L.; Lancellotti, I.; Karamanova, E.; Ranguelov, B.; Karamanov, A. Post-treated incinerator bottom ash as alternative raw material for ceramic manufacturing. *J. Eur. Ceram. Soc.* **2012**, *32*, 2843–2852. [CrossRef]
32. Chen, Z.; Liu, Y.; Zhu, W.; Yang, E. Incinerator bottom ash (IBA) aerated geopolymer. *Constr. Build. Mater.* **2016**, *1121*, 1025–1031. [CrossRef]

33. Wongsa, A.; Boonserm, K.; Waisurasingha, C.; Sata, V.; Chindaprasirt, P. Use of municipal solid waste incinerator (MSWI) bottom ash in high calcium fly ash geopolymer matrix. *J. Clean. Prod.* **2017**, *1481*, 49–59. [CrossRef]
34. Zhu, W.; Teoh, P.J.; Liu, Y.; Chen, Z.; Yang, E. Strategic utilization of municipal solid waste incineration bottom ash for the synthesis of lightweight aerated alkali-activated materials. *J. Clean. Prod.* **2019**, *23520*, 603–612. [CrossRef]
35. Chindaprasirt, P.; Jaturapitakkul, C.; Chalee, W.; Rattanasak, U. Comparative study on the characteristics of fly ash and bottom ash geopolymers. *Waste Manag.* **2009**, *29*, 539–543. [CrossRef]
36. Chindaprasirt, P.; Rattanasak, U. Utilization of blended fluidized bed combustion (FBC) ash and pulverized coal combustion (PCC) fly ash in geopolymer. *Waste Manag.* **2010**, *30*, 667–672. [CrossRef]
37. Topcu, I.B.; Toprak, M.U. Properties of geopolymer from circulating fluidized bed combustion coal bottom ash. *Mater. Sci. Eng. A* **2011**, *528*, 1472–1477. [CrossRef]
38. Xu, H.; Li, Q.; Shen, L.; Wang, W.; Zhai, J. Synthesis of thermostable geopolymer from circulating fluidized bed combustion (CFBC) bottom ash. *J. Hazard. Mater.* **2010**, *175*, 198–204. [CrossRef] [PubMed]
39. Noor-ul-Amin, S.; Faisal, M.; Muhammad, K.; Gul, S. Synthesis and characterization of geopolymer from bagasse bottom ash, waste of sugar industries and naturally available china clay. *J. Clean. Prod.* **2016**, *12915*, 491–495. [CrossRef]
40. Sata, V.; Sathonsaowaphak, A.; Chindaprasirt, P. Resistance of lignite bottom ash geopolymer mortar to sulfate and sulfuric acid attack. *Cem. Concr. Compos.* **2012**, *34*, 700–708. [CrossRef]
41. Nkuna, C.N.; Oboirien, B.O.; Sadiku, E.R.; Lekitima, J. A comparative study of geopolymers synthesized from OXY-combustion and chemical looping combustion bottom ashes. *Constr. Build. Mater.* **2017**, *1361*, 246–255. [CrossRef]
42. Khamlue, P.; Lertcumfu, N.; Jaita, P.; Manotham, S.; Tunkasiri, T.; Malasri, P.; Rujijanagul, G. The Effects of Biochar Additive on the Properties of Geopolymer Materials. *Key Eng. Mater.* **2019**, *798*, 273–278. [CrossRef]
43. Bai, C.; Colombo, P. Processing, properties and applications of highly porous geopolymers: A review. *Ceram. Int.* **2018**, *44*, 16103–16118. [CrossRef]
44. Farges, R.; Gharzouni, A.; Ravier, B.; Jeulin, P.; Rossignol, S. Insulating Foams and Dense Geopolymers from Biochar By-Products. *J. Ceram. Sci. Technol.* **2018**, *9*, 193–200.
45. Devi, P.; Saroha, A.K. Risk assessment and technical feasibility of usage of paper mill sludge biochar-based exhausted adsorbent for geopolymeric brick formation. *Environ. Sci. Pollut. Res.* **2016**, *23*, 21641–21651. [CrossRef]
46. Farzanian, K.; Teixeira, K.P.; Perdigao Rocha, I.; De Sa Carneiro, L.; Ghahremaninezhad, A. The mechanical strength, degree of hydration and electrical resistivity of cement pastes modified with superabsorbent polymers. *Constr. Build. Mater.* **2016**, *109*, 156–165. [CrossRef]
47. Schrofl, C.; Mechtcherine, V.; Gorges, M. Relation between the molecular structure and the efficiency of superabsorbent polymers (SAP) as concrete admixture to mitigate autogenous shrinkage. *Cem. Concr. Res.* **2012**, *42*, 865–873. [CrossRef]
48. Wang, A.; Sun, D.; Cao, G.; Wang, H.; Ren, N.; Wu, W.; Logan, B.E. Integrated hydrogen production process from cellulose by combining dark fermentation, microbial fuel cells, and a microbial electrolysis cell. *Bioresour. Technol.* **2011**, *102*, 4137–4143. [CrossRef] [PubMed]
49. Devi, P.; Saroha, A.K. Effect of Temperature on Biochar Properties during Paper Mill Sludge Pyrolysis. *Int. J. Chem. Tech. Res.* **2013**, *5*, 682–687. Available online: https://www.researchgate.net/profile/Parmila_Devi/publication/259449899_Effect_Of_Temperature_On_Biochar_Properties_During_Paper_Mill_Sludge_Pyrolysis/links/0deec53637ec17aae7000000.pdf (accessed on 10 November 2021).
50. Bedussi, F. Evaluation of the Potential of Biochar as a Component of Cultivation Substrates. Ph.D. Thesis, Department of Agricultural and Environmental Sciences, University of Milan, Milan, Italy, 2015.
51. Brewer, C.; Chuang, V.J.; Masiello, C.A.; Gonnermann, H.; Gao, X.; Dugan, B.; Driver, L.E.; Panzacchi, P.; Zygourakis, K.; Davies, C.A. New approaches to measuring biochar density and porosity. *Biomass Bioenergy* **2014**, *66*, 176–185. [CrossRef]
52. Kiventera, J.; Lancellotti, I.; Catauro, M.; Dal Poggetto, F.; Leonelli, C.; Illikainen, M. Alkali activation as new option for gold mine tailings inertization. *J. Clean. Prod.* **2018**, *187*, 76–84. [CrossRef]
53. Webb, P.; Orr, C. *Analytical Methods in Fine Particle Technology*; Micromeritics Instrument Corp.: Norcross, GA, USA, 1997.